with T-tubule abnormalities [38], but most of caveolin-3 in the adult stage has been found at the sarcolemma by immunohistochemistry [37]. Caveolin-3 has also been reported to participate in an insulin-regulated transport mechanism in muscle [33]. Under activation, caveolin-3-containing vesicles traffic between intracellular sites and target sites on the sarcolemma and T-tubules. Not much is known about the precise nature of how caveolin-3 associates with T-tubules. However, based on our finding, it would be intriguing to assume that dysferlin might be involved in the fusion of caveolin-3-containing vesicles with T-tubules.

On the basis of immunohistochemical finding that dysferlin is present in the cytoplasm [12,16], it has been proposed that dysferlin-carrying vesicles participate in the injury-induced membrane repair of the sarcolemma [17]. However, our present findings suggest that the cytoplasmic staining does not always show the presence of such vesicles, since at least a portion was contributed by T-tubule-associated dysferlin. Evaluation of the proposed model, together with identification of the dysferlin-carrying membrane vesicles, should be encouraged by further studies.

In conclusion, we have shown by systematic subcellular membrane fractionation that dysferlin associates with both sarcolemma- and T-tubule-enriched membrane fractions. The latter was consistent with our demonstrated interaction of dysferlin with DHPR. We have also shown an association between DHPR and the dysferlin-interacting protein caveolin-3, raising the possibility that dysferlin may form an oligomeric complex. Two not yet identified WGA-binding proteins, 80 and 100 kDa, may participate in this complex. Our findings suggest that dysferlin might play role(s) other than the putative injury-induced membrane repair.

Acknowledgements

The authors would like to thank Mr. Satoru Masuda for his support during the course of this research. This work was supported by Research Grants (14B-4 and 17A-10) for Nervous and Mental Disorders (to MY), Health Sciences Research grants for Research on Psychiatric and Neurological Diseases and Mental Health (H12-kokoro-025, H15-kokoro-021) from the Ministry of Health, Labor and Welfare, a Grant-in-Aid for Scientific Research from the Ministry of Education, Science, Sports and Culture of Japan (to ST) and the Atsumi Foreign Students Scholarship Foundation, Tokyo, Japan (to BNA).

Abbreviations

C. elegans, Caenorabditis elegans; DHPR, the dihydropyridine receptor; EGTA, O, O'-bis(2-aminoethyl)ethyleneglycol-N, N, N', N'-tetraacetic acid; LGMD 2B, limb girdle muscular dystrophy 2B; NaK-ATPase, sodium potassium ATPase; RyR, ryanodine receptor; SR, the sarcoplasmic reticulum; T-tubules, transverse tubules; SERCA, sarco/endoplasmic reticulum calcium ATPase; WGA, wheat germ agglutinin.

References

1. Miyoshi K, Kawai H, Iwasa M, et al. Autosomal recessive distal muscular dystrophy as a new type of progressive muscular dystrophy. Seventeen cases in eight families including an autopsied case. Brain 1986;109:31–54.
2. Bashir R, Strachan T, Keers S, et al. A gene for autosomal recessive limb-girdle muscular dystrophy maps to chromosome 2p. Hum Mol Genet 1994;3:455-7.
3. Galassi G, Rowland LP, Hays AP, et al. High serum levels of creatine kinase: asymptomatic prelude to distal myopathy. Muscle Nerve 1987;10:346-50.
4. Liu J, Aoki M, Illa I, et al. Dysferlin, a novel skeletal muscle gene, is mutated in Miyoshi myopathy and limb girdle muscular dystrophy. Nature Genet 1998;20:31-6.
5. Bashir R, Britton S, Strachan T, et al. A gene related to Caenorhabditis elegans spermatogenesis factor fer-1 is mutated in limb-girdle muscular dystrophy type 2B. Nature Genet 1998;20:37-42.
6. Rizo J, Sudhof TC. C2 domains, structure and function of a universal binding domain. J Biol Chem 1998;273:15879-82.
7. Li C, Ullrich B, Zhang JZ, et al. Ca(2+)-dependent and -independent activities of neural and non-neural synaptotagmins. Nature 1995; 375: 594-9.
8. Perin MS, Fried VA, Mignery GA, et al. Phospholipid binding by a synaptic vesicle protein homologous to the regulatory region of protein kinase C. Nature 1990; 345: 260-3.
9. Davis DB, Delmonte AJ, Ly CT, et al. Myoferlin, a candidate gene and potential modifier of muscular dystrophy. Hum Mol Genet 2000;9:217-26.
10. Yasunaga S, Grati M, Cohen-Salmon M, et al. A mutation in OTOF, encoding otoferlin, a FER-1-like protein, causes DFNB9, a nonsyndromic form of deafness. Nature Genet. 1999; 21: 363-9.
11. Achanzar WE, Ward S. A nematode gene required for sperm vesicle fusion. J Cell Sci 1997;110:1073-81.
12. Bansal D, Miyake K, Vogel SS, et al. Defective membrane repair in dysferlin-deficient muscular dystrophy. Nature 2003;423:168-72.
13. Lennon NJ, Kho A, Bacskai BJ, et al. Dysferlin interacts with annexins A1 and A2 and mediates sarcolemmal wound-healing. Biol. Chem. 2003;278:50466-73.
14. Anderson LV, Davison K, Moss JA, et al. Dysferlin is a plasma membrane protein and is expressed early in human development. Hum Mol Genet 1999;8:855-61.

15. Matsuda C, Aoki M, Hayashi YK, et al. Dysferlin is a surface membrane-associated protein that is absent in Miyoshi myopathy. Neurol 1999;53:1119-22.
16. Piccolo F, Moore SA, Ford GC, et al. Intracellular accumulation and reduced sarcolemmal expression of dysferlin in limb-girdle muscular dystrophies. Ann Neurol. 2000;48:902-12.
17. Bansal D, Campbell KP. Dysferlin and the plasma membrane repair in muscular dystrophy. Trends Cell Biol 2004;14:206-13.
18. Bittner RE, Anderson LVB, Burkhardt E, et al. Dysferlin deletion in SJL mice (SJL-Dysf) defines a natural model for limb girdle muscular dystrophy 2B. Nature Genet 1999;23:141-2.
19. Vafiadaki E, Reis A, Keers S, et al. Cloning of the mouse dysferlin gene and genomic characterization of the SJL-Dysf mutation. Neuroreport 2001;12:625-9.
20. Tokuue Y, Goto S, Imamura M, et al. Transfection of chicken skeletal muscle α-actinin cDNA into nonmuscle and myogenic cells: dimerization is not essential for α-actinin to bind to microfilaments. Exp Cell Res 1991;197:158-67.
21. Dombrowski L, Roy D, Marcotte B, et al. A new procedure for the isolation of plasma membranes, T tubules, and internal membranes from skeletal muscle. Am J Physiol 1996;270:E667-76.
22. Munoz P, Rosemblatt M, Testar X, et al. Isolation and characterization of distinct domains of sarcolemma and T-tubules from rat skeletal muscle. Biochem J 1995; 307:273-80.
23. Yoshida M, Ozawa E. Glycoprotein complex anchoring dystrophin to sarcolemma. J Biochem 1990;108:748-52.
24. Kyhse-Anderson J. Electroblotting of multiple gels: a simple apparatus without buffer tank for rapid transfer of proteins from polycrylamide to nitrocellulose J Biochem Biophys Methods.1984;10:203-9.
25. Matsuda C, Hayashi YK, Ogawa M, et al. The sarcolemmal proteins dysferlin and caveolin-3 interact in skeletal muscle. Hum Mol Genet 2002;10:1761-6.
26. Jahn R, Sudhof TC. Membrane fusion and exocytosis. Annu Rev Biochem 1999;68:863-911.
27. Matsuda C, Kameyama K, Tagawa K, et al. Dysferlin interacts with affixin (beta-parvin) at the sarcolemma. J Neuropathol Exp Neurol 2005;64:334-40.
28. Ervasti JM, Ohlendieck K, kahl SD, et al. Deficiency of a glycoprotein component of the dystrophin complex in dystrophic muscle. Nature 1990;345:319-25.
29. Campbell KP, Leung AT, Sharp AH. The biochemistry and molecular biology of the dihydropyridine-sensitive calcium channel. Trends Neurosci 1988;11:425-30.
30. Flucher BE. Structural analysis of muscle development: transverse tubules, sarcoplasmic reticulum, and the triad. Dev Biol 1992;154:245-60.
31. Ursu D, Sebille S, Dietze B, et al. Excitation-contraction coupling in skeletal muscle of a mouse lacking the dihydropyridine receptor subunit gamma1. J Physiol 2001;533:367-77.
32. Ahern CA, Vallejo P, Mortenson L, et al. Functional analysis of a frame-shift mutant of the dihydropyridine receptor pore subunit (alpha1S) expressing two complementary protein fragments. BMC Physiol 2001;1:1-11.
33. Munoz P, Mora S, Sevilla L, et al. Expression and insulin-regulated distribution of caveolin in skeletal muscle. Caveolin does not colocalize with GLUT4 in intracellular membranes. J Biol Chem 1996;271:8133-9.
34. Rothberg KG, Heuser JE, Donzell WC, et al. Caveolin, a protein component of caveolae membrane coats. Cell 1992;68:673-82.
35. Fujimoto T. Calcium pump of the plasma membrane is localized in caveolae. J Cell Biol 1993;120:1147-57.
36. Lisanti MP, Scherer PE, Tang Z, et al. Caveolae, caveolin and caveolin-rich membrane domains: a signaling hypothesis. Trends Cell Biol 1994;4:231-35.
37. Parton RG, Way M, Zorzi N, et al. Caveolin-3 associates with developing t-tubules during muscle differentiation. J Cell Biol 1997;136:137-54.
38. Galbiati F, Engelman JA, Volonte D, et al. Caveolin-3 null mice show a loss of caveolae, changes in the microdomain distribution of the dystrophin-glycoprotein complex, and T-tubule abnormalities. J Biol Chem 2001;276:21425-33.

Acta Myologica • 2005; XXIV: p. 145-154

Major clinical and histopathological characteristics of canine X-linked muscular dystrophy in Japan, CXMD$_J$

YOSHIKI SHIMATSU[1], MADOKA YOSHIMURA[1], KATSUTOSHI YUASA[1], NOBUYUKI URASAWA[1], MASAYUKI TOMOHIRO[1], MASAO NAKURA[2], MANABU TANIGAWA[2], AKINORI NAKAMURA[1], SHIN'ICHI TAKEDA[1]

[1]*Department of Molecular Therapy, National Institute of Neuroscience, National Center of Neurology and Psychiatry, 4-1-1 Ogawa-higashi, Kodaira, Tokyo 187-8502, Japan*
[2]*Chugai Research Institute for Medical Science, Inc., 6598 Toyoda, Suwa, Nagano 392-0016, Japan*

Canine X-linked muscular dystrophy (CXMD), which was found in a colony of golden retriever, is caused by a mutation in the *dystrophin* gene and it is a useful model of Duchenne muscular dystrophy (DMD). To investigate the pathogenesis and to develop therapy of DMD, we have established a beagle-based CXMD colony in Japan (CXMD$_J$) and examined their phenotypes. The mortality by 3 days of age in the third generation (G3) of CXMD$_J$ dogs, 32.3%, was considerably higher than that in normal G3 littermates, 13.3%. Serum creatine kinase (CK) levels of G3 CXMD$_J$ were significantly higher than that of normal male dogs with two peaks: at shortly after birth and around 2 months of age. Diaphragm muscle involvement occurred shortly after birth and was more severe than that of limb muscles. Stress during whelping might be associated with the neonatal death and respiratory muscle involvement. Gait disturbance was also noticed after 2 months of age. The involvement of limb and temporal muscles was observed from 2 months of age, which corresponded with the second peak of serum CK. Macroglossia, dysphagia, drooling and jaw joint contracture were overt from 4 months of age. We noticed severe macroglossia and hypertrophy of the sublingual muscles at the age of 12 months, and these were important features of this model, because dysphagia is one of major symptoms in older DMD patients. Overall, the phenotypes of CXMD$_J$ were roughly identical to those of CXMD dogs in the literature. Beagle-based CXMD$_J$ is smaller and easier to handle than golden retriever, therefore they are a useful model for DMD.

Key words: Canine X-linked muscular dystrophy; dystrophin; creatine kinase

Introduction

Duchenne muscular dystrophy (DMD) is an X-linked recessive disease characterized by skeletal muscle atrophy and weakness [1], and is caused by mutations in the *dystrophin* gene [2]. DMD patients exhibit muscle weakness by 2 to 5 years of age, are unable to walk, and die by their twenties as a result of either respiratory or cardiac failure [1]. Recently the prognosis of patients suffering from DMD has been greatly improved by the use of respirators.

In research on the molecular pathogenesis of dystrophin deficiency, *mdx* mice have been frequently used as an experimental model, but the clinical symptoms of *mdx* mice are much milder than those of patients suffering from DMD [3]. Another model for DMD, canine X-linked muscular dystrophy (CXMD), which was found in a golden retriever, lacks dystrophin, and reveals clinical and pathological findings that are more similar to those of DMD [4-7]. Therefore, CXMD dogs are more appropriate than *mdx* mice as an animal model [5, 7, 8], although a severely affected animal model is difficult to raise and handle.

We established a beagle-based colony of CXMD dogs in Japan designated CXMD$_J$ [9]. The first generations (G1) of carrier female dogs were produced by artificial insemination of a beagle bitch with frozen semen derived from a CXMD, and the second generation (G2) and the third generation (G3) of CXMD$_J$ dogs were born to interbreed G1 and G2 carrier female dogs and beagle sires, respectively.

CXMD is a very important experimental model for the development of therapies for dystrophin deficiency. The efforts that have been made to

Address for correspondence: Shin'ichi Takeda, M.D., Ph.D., Department of Molecular Therapy, National Institute of Neuroscience, National Center of Neurology and Psychiatry, 4-1-1 Ogawa-higashi, Kodaira, Tokyo 187-8502, Japan. Fax: +81-42-346-1750. E-mail: takeda@ncnp.go.jp

explore experimental therapies in *mdx* mice may also be applicable to a large animal model such as CXMD in the future. These efforts include pharmaceuticals [10], gene transfer [11], or cell transplantation therapy [12]. Very recently hematopoietic cell transplantation has been tried using CXMD [13]. In this report, the major phenotypes of G3 $CXMD_J$ dogs were investigated and compared with those of CXMD dogs. We found that $CXMD_J$ dogs are a suitable model to develop therapies for DMD.

Materials and Methods

Animals

All dogs were part of the $CXMD_J$ breeding colony at the General Animal Research Facility, National Institute of Neuroscience, National Center of Neurology and Psychiatry (Tokyo, Japan) or Chugai Research Institute for Medical Science, Inc. (Nagano, Japan) [9]. Seven G2 carrier females were mated with normal beagle sires or inseminated with fresh normal beagle semen. Ninety-nine G3 pups were produced by 12 whelpings of G2 carriers. The genotypes of the pups were analyzed by Snapback SSCP [14]. Forty-five male and female littermates were normal, 31 male pups were affected, and 23 female pups were carriers. We analyzed affected G3 males together with normal G3 male and female littermates, and carrier G3 females in this study.

A pregnant carrier G2 female was removed to stainless steel cage for whelping (1,580 x 1,580 x 930 mm) at 7 days before the expected whelping day. The carrier female nursed G3 pups after her whelping, and the weaning of pups was done at 6 weeks after birth. Affected G3 pups were then individually housed in the cages (1,700 x 960 x 1,570 mm), but the remaining pups were fed with 2 or 3 pups in the same largeness of cages up to around 3 months of age. All dogs were given a mixture of soaking pellet with synthetic powdered milk up to 3 months of age, and then given a pellet diet. They also had *ad libitum* access to filtered water. The room temperature was maintained at 22 ± 2°C, and the relative humidity was 40-70%. A veterinarian examined the healthy care of the dogs once a week. All dogs in this experiment were treated in accordance with the guidelines provided by the Ethics Committee for Treatment of Laboratory Middle-Sized Animals of the National Institute of Neuroscience, National Center of Neurology and Psychiatry (Tokyo, Japan) or the Ethics Committee for Treatment of Laboratory Animals of Chugai Pharmaceutical Co., Ltd. (Tokyo, Japan).

Death by 3 days of age

The rates of death by 3 days of age were calculated in 31 affected G3 male pups and 45 normal G3 male and female pups, respectively.

Body weight

The body weight of normal (n = 4) and affected (n = 8) G3 males were measured at every second day from 1 to 21 days, and at 1.5, 2, 4, 6, 8, 10, and 12 months of age. Synthetic milk was given through tube for 14 days to four affected G3 pups whose body weight at 3 days of age was decreased than that of 1 day after birth.

Serum creatine kinase (CK) levels

Blood samples of normal male (n = 5), female (n = 3 before 2 months of age, n = 2 at 3 months of age), affected male (n = 8), and carrier female (n = 4) G3 dogs were obtained by cephalic or jugular venipuncture at 1 day, 3 weeks, and 1.5, 2, 3, 6, and 12 months of age. Serum CK levels were assayed using an automated colorimetric analyzer (FDC3500, FujiFilm Medical, Tokyo, Japan).

Clinical manifestations

We observed gait and mobility disturbances, involvement of limb, temporal, and tongue muscles, dysphagia, and drooling as clinical signs in normal (n = 5) and affected (n = 5) G3 males at the ages of 1, 2, 4, 6, and 12 months. The severity of each sign was classified according to a new grading scale for the $CXMD_J$ colony (**Table**) based on both a previous report [15] and a clinical record prepared for an Australian CXMD colony by J.M. Howell et al. (personal communication). We also measured the maximum mouth opening to evaluate the jaw joint contracture. At least one veterinarian and two medical doctors who are very familiar with symptoms of dystrophic dogs did all clinical examinations.

Macroscopic and histopathological examinations

Muscle samples from normal (n = 5) and affected (n = 5) G3 males were obtained when

Table 1. Grading of clinical signs in $CXMD_J$ dogs.

Gait disturbance	
Grade	1: None
Grade	2: Sitting with hind legs extended
Grade	3: Bunny hops with hind legs
Grade	4: Shuffling walk
Grade	5: Unable to walk
Mobility disturbance	
Grade	1: None
Grade	2: lying down more than normal
Grade	3: Cannot jump on hind legs
Grade	4: Increasing difficulty moving around
Grade	5: Unable to get up and move around
Limb or temporal muscle atrophy	
Grade	1: None
Grade	2: Suspect hardness
Grade	3: Can feel hardness or apparently thin
Grade	4: Between Grade 3 and 5
Grade	5: Extremely thin or hard
Drooling	
Grade	1: None
Grade	2: Occasionally dribbles saliva when sitting
Grade	3: Some drool when eating and drinking
Grade	4: Strings of drool when eating or drinking
Grade	5: Continuous drool
Macroglossia	
Grade	1: None
Grade	2: Slightly enlarged
Grade	3: Extended outside dentition
Grade	4: Enlarged and slightly thickened
Grade	5: Enlarged and thickened
Dysphagia	
Grade	1: None
Grade	2: Takes time and effort in taking food
Grade	3: Difficulty in taking food from plate
Grade	4: Difficulty in chewing, swallowing or drinking
Grade	5: Unable to eat

These grading scales were developed at our institute on the basis of a previous report [15] and a personal communication with J.M. Howell et al. in Australia.

the dogs died at 1 day of age or were sacrificed at the ages of 3 days and 2, 6, and 12 months by using an overdose of intravenous pentobarbital. Some portions of the diaphragm and anterior tibial muscles were snap-frozen in cooled isopentane, and cryostat sections (6 μm) were stained with hematoxylin and eosin (H&E). The tongue, genioglossus, and geniohyoideus muscles were fixed in 15% neutral buffered formalin, embedded in paraffin, and 6 μm sections were stained with H&E.

Statistical analysis

The data of body weight, serum CK level, and the maximum mouth opening were subjected to a one-way analysis of variance test. Fisher's protected least significant difference test was used for post-hoc comparisons. The statistical significance of the pup death rate was evaluated using the chi-square test. All values are expressed as mean ± standard error (S.E.). A p value of less than 0.05 was considered to indicate statistical significance. All calculations were performed using StatView software (SAS Institute, Cary, NC, USA).

Results

Death by 3 days of age

Ten of 31 G3 $CXMD_J$ pups died, a death rate of 32.3%. Among normal G3 male and female pups, six out of 45 (13.3%) died. The ratio of affected G3 pups was significantly higher than that of normal pups ($p < 0.05$). We did not find any dead pups from 4 days to 4 weeks of age during the lactation period.

Body weight

Body weight changes of G3 male dogs (4 normal and 4 affected without tube feeding) in the $CXMD_J$ colony are shown in **Fig. 1A**. Affected G3 males showed retardation in increase of body weight after 6 months of age and the difference between them was statistically significant at the age of 10 and 12 months (**Fig. 1A**). While, the body weight of affected G3 male pups needed tube feeding was significantly lower than that of either normal or affected G3 male without tube feeding at 5, 7, and 9 days of age (**Fig. 1B**). The difference in body weight between normal and carrier G3 females was not seen from 1 day to 6 months of age (data not shown).

Serum CK levels

Changes of serum CK levels of dogs in the $CXMD_J$ colony are shown in **Fig. 2**. The values of normal G3 males and females ranged from 80 to 4,000 IU/l up to 12 months of age. The difference in the CK levels between normal and affected G3 males was statistically significant at every age examined. The average serum CK level made a biphasic pattern: it was 120,000 IU/l at 1 day of age and then had decreased to 11,000 IU/l at 3

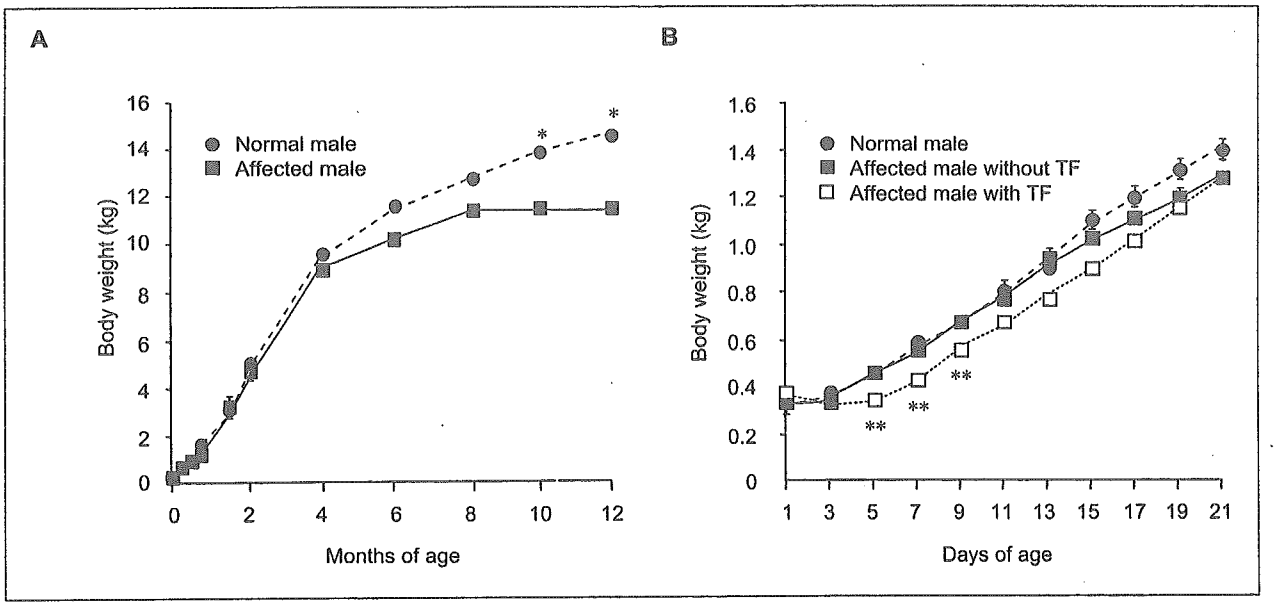

Figure 1. (**A**) Body weight changes up to 12 months of normal and affected G3 male dogs in $CXMD_J$ colony. (**B**) Body weight changes of G3 male dogs of normal, affected without tube feeding (TF), and affected with TF up to 21 days. Bar: mean ± S.E.; $^{**}p < 0.01$; $^{*}p < 0.05$.

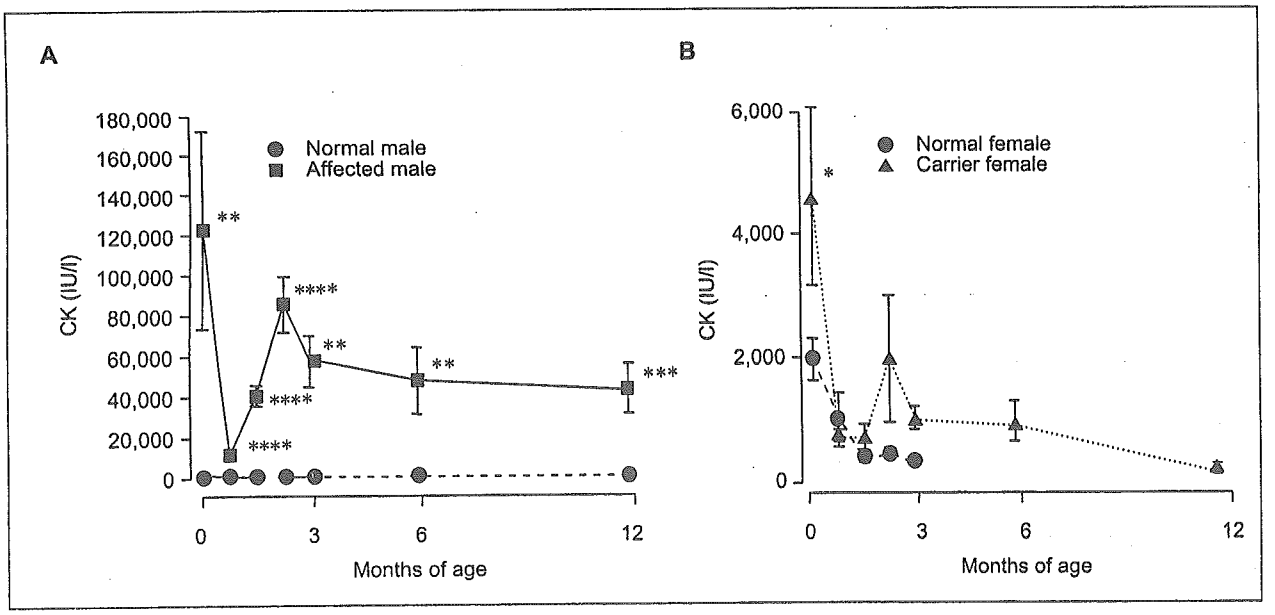

Figure 2. Serum CK levels of G3 dogs in $CXMD_J$ colony in (**A**) normal and affected males and (**B**) normal and carrier females. Bar: mean ± S.E.; $^{****}p< 0.0001$; $^{***}p < 0.001$; $^{**}p < 0.01$; $^{*}p < 0.05$.

weeks of age (**Fig. 2A**); however, the levels had increased again to 85,000 IU/l at 2 months of age, and then the values gradually decreased. Like affected G3 males, the serum CK levels in carrier G3 females, both at 1 day and 2 months of age, were higher than those in normal G3 females, and the difference at 1 day of age was statistically significant (**Fig. 2B**).

Clinical manifestations

In CXMD male dogs at 14 months of age, kyphosis and atrophy of temporal, truncal, and limb muscles were observed; many muscles, especially the proximal limb muscles, were firm on palpation [15]. A representative G3 $CXMD_J$ male dog at 12 months of age had signs similar to those described above (**Fig. 3**). Moreover, CXMD dogs

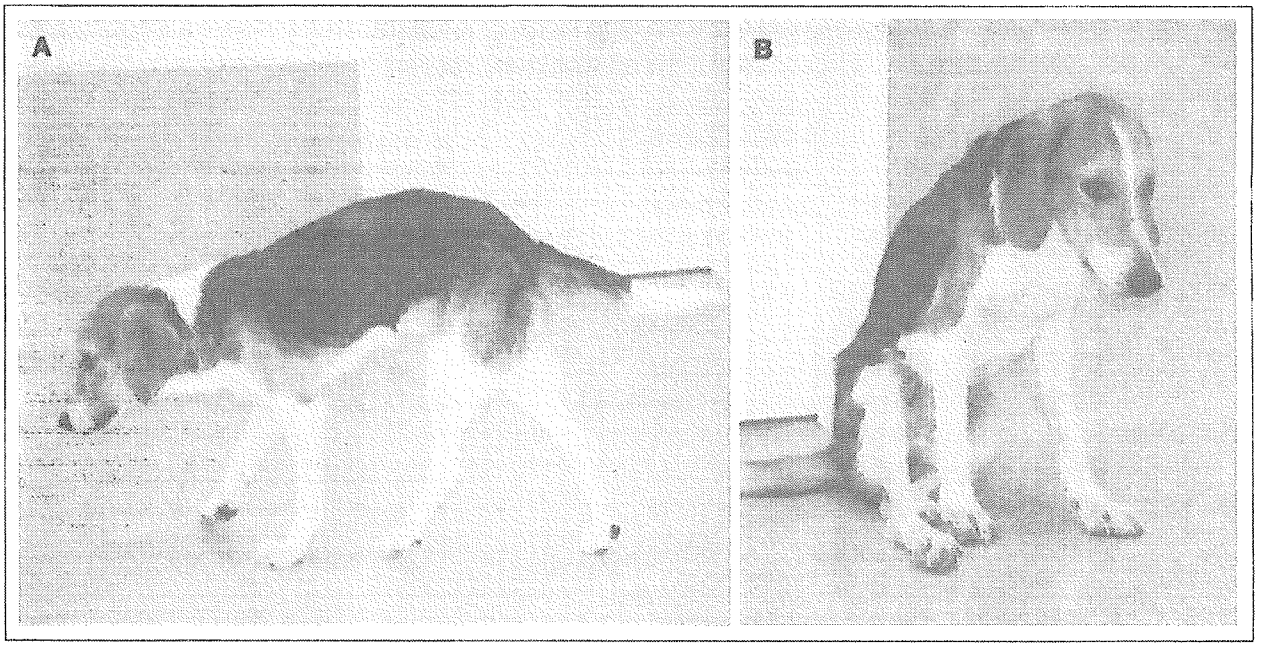

Figure 3. A representative affected G3 male dog at 12 months of age.
(**A**) When walking, spine curvature, supinate front paws, and drop feet in hind limbs were observed.
(**B**) Severe temporal muscle atrophy and throwing of hind limbs when sitting were recognized.

showed gait and mobility disturbances, and progressive tongue enlargement, dysphagia, feeding difficulty, and excessive salivation were also recognized [15]. We, therefore, evaluated the clinical phenotypes of affected G3 male dogs at the ages of 1, 2, 4, 6, and 12 months.

Within a week after the birth, affected pups were slightly less active than normal littermates during the period. Around 2 months of age, dystrophic pups sometimes sit with hind legs extended. The dog showed stiff limbs, but these symptoms were probably related to contraction of the joints. Soon after, they move the hind limbs simultaneously (bunny-hops with hind legs) (**Fig. 4A and B**). Distal limb muscle atrophy appeared from 2 months of age in the dogs (**Fig. 4C**), but proximal limb muscle atrophy in G3 males was observed at 4 months of age (**Fig. 4D**). Proximal limb muscle, especially thigh muscle, has been spared at the relatively early period, but that was severer than distal limb muscle atrophy at 12 months of age (**Fig. 3A**). The temporal muscle was also involved at the age of 2 months, and it was much more atrophied than other muscles at the age of 12 months (**Fig. 3B and 4E**). Around 4 months of age, they occasionally dribbled saliva when sitting. They frequently showed tongue hypertrophy (**Fig. 4F and G**), and inability to open the jaw due to contracture of the joints. 40% of dogs showed difficulty in eating food or swallowing at the age of 6 months (**Fig. 4H**), therefore hand feeding is sometimes required for the dogs. An enlarged and thickened tongue was seen in all affected G3 males at 12 months of age. To ascertain the degree of jaw joint contracture, we examined the maximum mouth opening in both normal and affected G3 males (**Fig. 4I**). The extent of the opening in normal G3 males increased with age, but it did not change much in the affected G3 dogs. The difference between them was significant at 4, 6, and 12 months of age, therefore jaw joint contracture probably started around 4 months of age in G3 affected dogs.

Macroscopic and histopathological findings

The diaphragm muscle of a normal G3 male that died at 1 day of age did not show streaks in the muscular portions (**Fig. 5A**): however, there were many radiating white streaks in an affected G3 male that died at 1 day of age (data not shown) as well as in another affected G3 male that was sacrificed at 3 days of age (**Fig. 5D**). Histopathological examination of the diaphragm muscle in a sacrificed, affected G3 male at 3 days of age showed acute stage of diffuse muscle necrosis with edema (**Fig. 5E**). At the age of 6 months, the

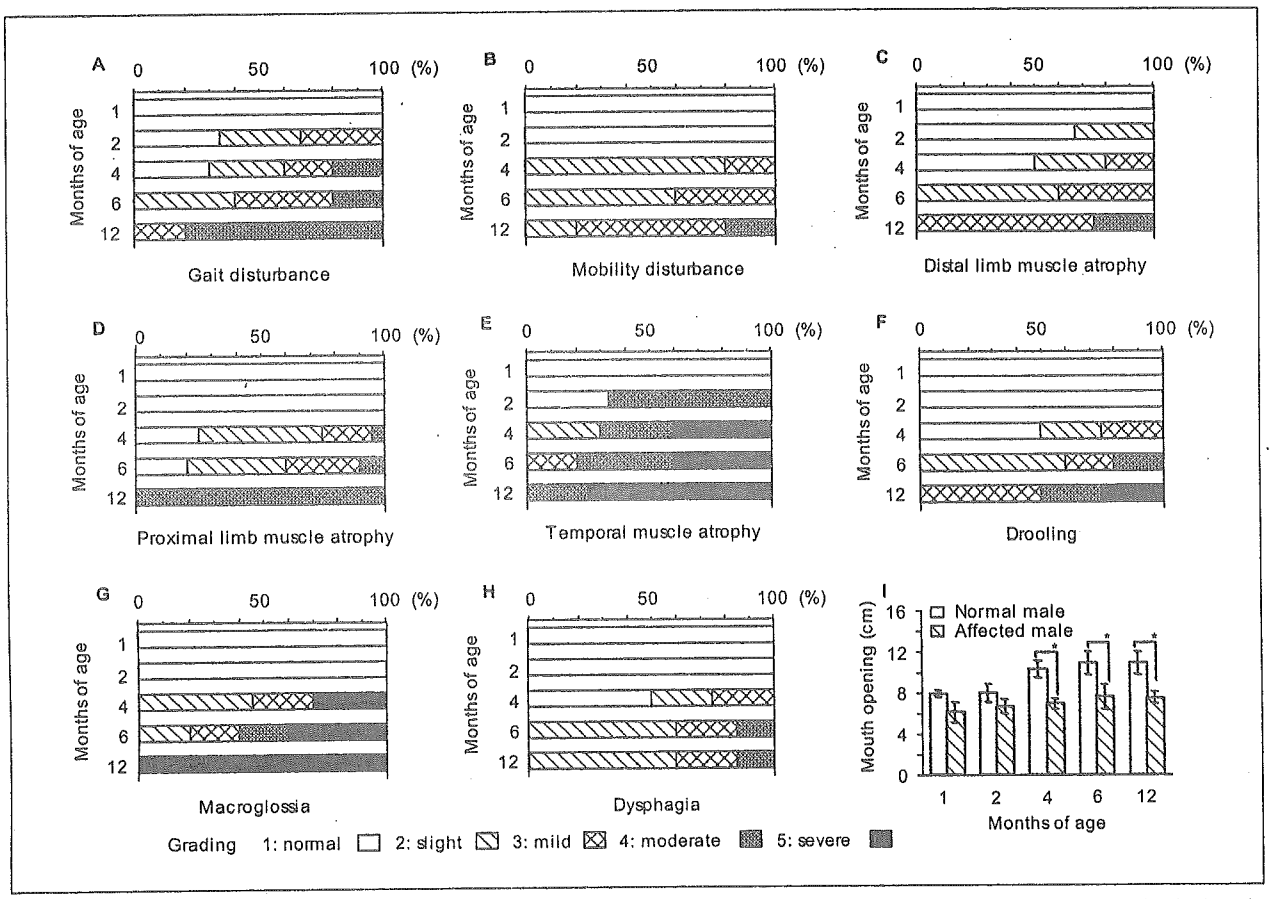

Figure 4. Evaluation of clinical phenotypes in affected G3 male dogs. The evaluation of each clinical sign is shown in **A-H**: (**A**) gait disturbance, (**B**) mobility disturbance (**C**) distal limb, (**D**) proximal limb, (**E**) and temporal muscle atrophy, (**F**) drooling, (**G**) macroglossia, and (**H**) dysphagia at the ages of 1, 2, 4, 6, and 12 months. The severity of each sign in affected G3 dogs was classified into five grades as described in Materials and Methods and Table. The percentage of affected G3 dogs in each grade was calculated for each month of age. (**I**) Maximum mouth opening in normal and affected G3 male dogs at the ages of 1, 2, 4, 6, and 12 months. Bar: mean ± S.E.; $^*p < 0.05$.

diaphragma muscle in an affected G3 male disclosed marked variation in fiber size and increase in fibrosis and necrotic fibers (**Fig. 5F**).

The diameter of the fibers in the anterior tibial muscle increased with age in normal G3 males (**Fig. 6A-C**), while the muscle in the sacrificed, affected G3 male at 3 days of age showed slight fiber size variation and some necrotic fibers (**Fig. 6D**). The findings were not different from those in an affected G3 male that died at 1 day of age (data not shown). At the age of 2 months, the tibial muscle from an affected G3 male displayed an increase in the number of necrotic fibers, invasion of inflammatory cells, and a slight proliferation of the interstitial tissues (**Fig. 6E**). At the age of 6 months, marked fiber size variation, increase in the interstitial fibrosis, and hypertrophied or centrally nucleated fibers were observed (**Fig. 6F**).

In macroscopic examinations, an affected G3 male at the age of 12 months had severe hypertrophy of the tongue, genioglossus, and geniohyoideus muscles (**Fig. 7B**) as compared with those in a normal male (**Fig. 7A**). In the tongue muscle, there were many hypertrophied fibers and opaque fibers (**Fig. 7D**), as compared with those in the normal male (**Fig. 7C**).

Discussion

In this report, we described the major clinical and histopathological phenotypes of beagle-based dystrophic dogs, $CXMD_J$, that carried the same *dystrophin* gene mutation as CXMD dogs. We

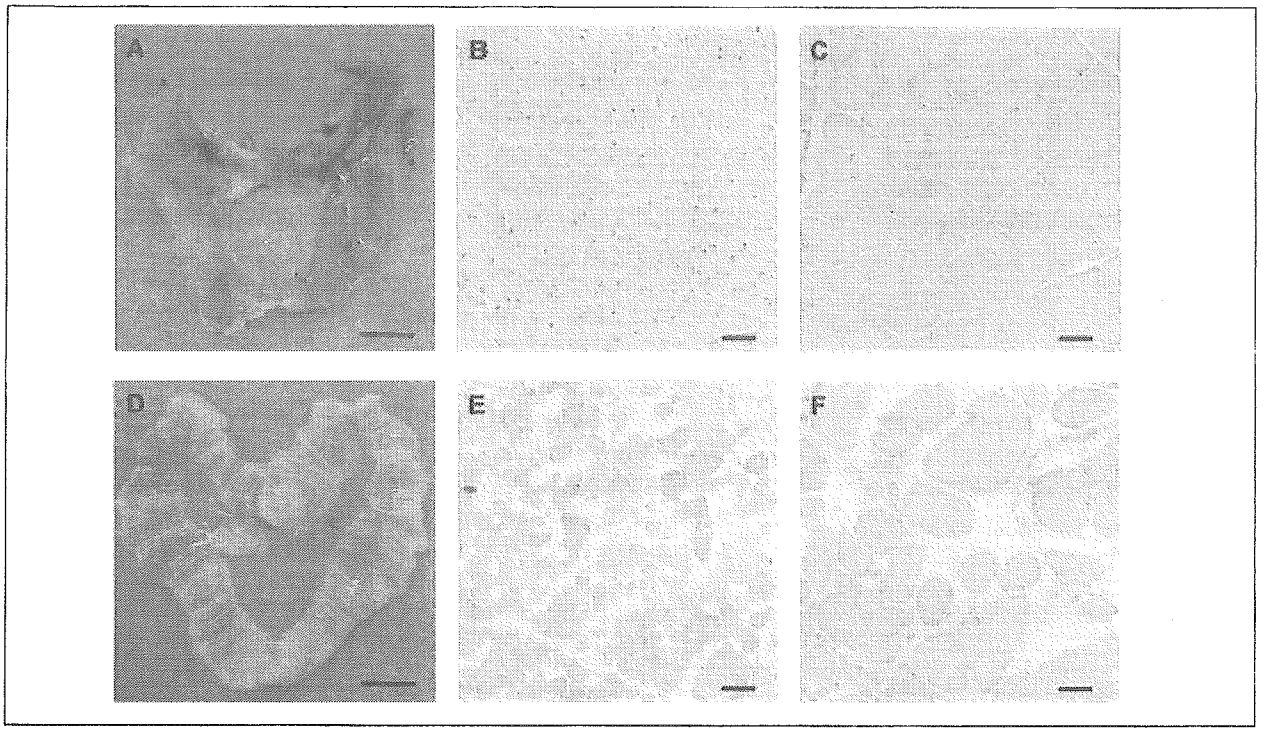

Figure 5. Macroscopy and histopathology of diaphragm muscles. Diaphragm of a normal G3 male dog that died at 1 day of age (**A**) and an affected G3 male dog that was sacrificed at 3 days of age (**D**). Bar = 1 cm. H&E staining of cross-sections of diaphragm muscles from normal G3 male at 3 day of age (**B**) and at 6 months of age (**C**), and from affected G3 males that was sacrificed at 3 days of age (**E**) and 6 months of age (**F**). Bar = 50 µm.

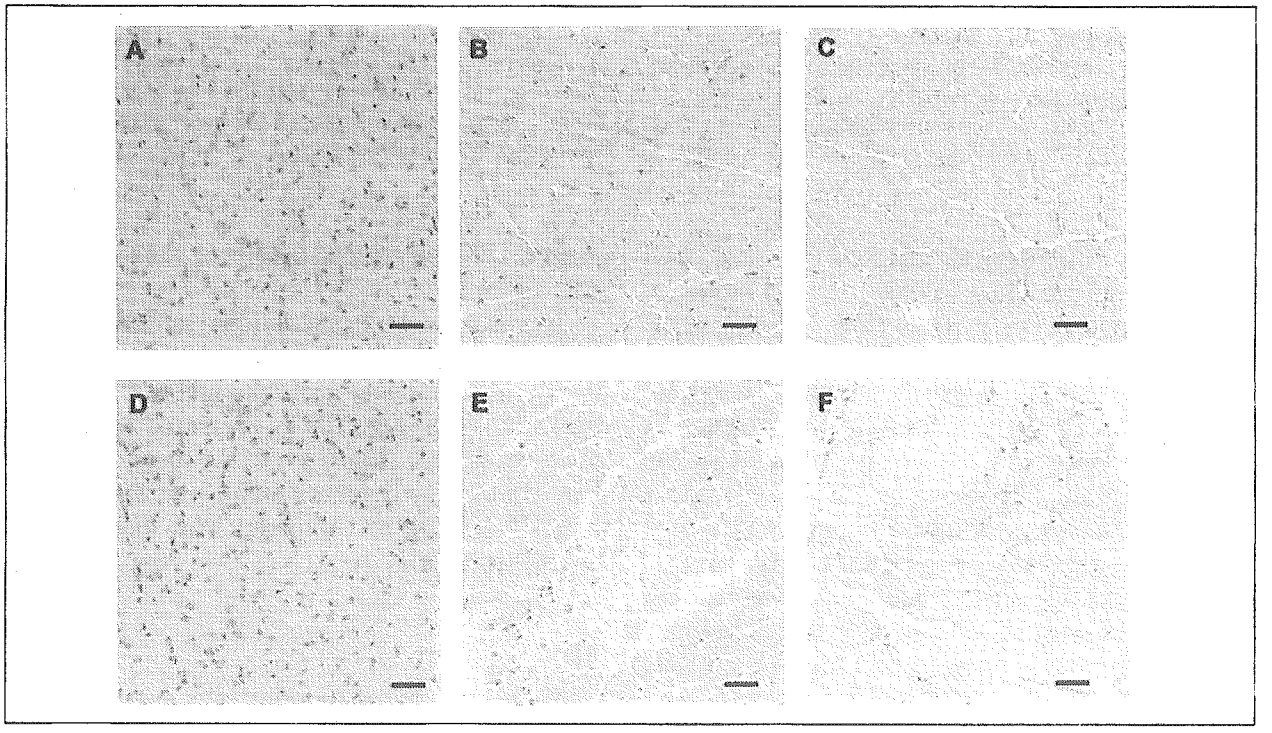

Figure 6. Histopathology of anterior tibial muscles. H&E staining of cross-sections of anterior tibial muscles from normal G3 male at 3 days of age (**A**), 2 month of age (**B**), and 6 months of age (**C**), and from affected G3 male at 3 days of age (**D**), 2 month of age (**E**), and 6 months of age (**F**). Bar = 50 µm

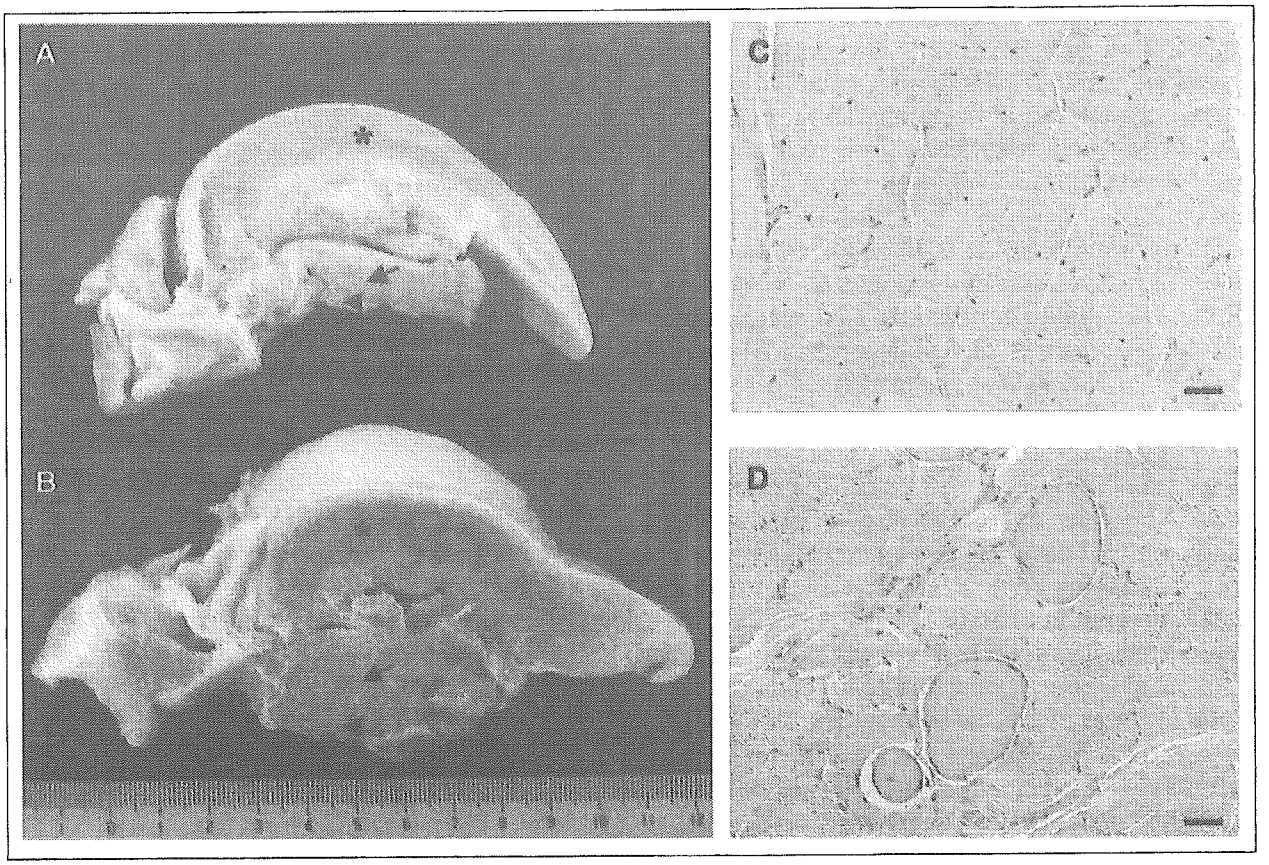

Figure 7. Macroscopy and histopathology of tongue and sublingual muscles. Tongue (asterisk), genioglossus (arrow) and geniohyoideus (arrowhead) muscles in a normal G3 male (**A**) and an affected G3 male (**B**) at 12 months of age. Bar = 1 cm. H&E staining of cross-sections of the tongue muscle from a normal G3 male (**C**) and an affected G3 male (**D**) at 12 months of age. Bar = 50 μm.

dealt mainly with the third generation of dystrophic dogs, G3, when they still have mixture of both beagle and golden retriever backgrounds. However, the size of G3 $CXMD_J$ was smaller and easier to handle than golden retriever-based CXMD dogs [16].

The serum CK levels in affected G3 dogs reached two peaks during the course: the first peak occurred immediately after birth and the second peak at two months after birth. This particular pattern of serum CK levels was also seen in G3 carrier females, although the increase was quite small. Previous researchers have reported that serum CK levels in CXMD dogs were much higher than those in normal littermates shortly after birth [15, 17] and had another peak at 6 to 8 weeks after birth [15]. The profiles of serum CK levels in our dystrophic G3 dogs corresponded well with these reports.

The elevation of serum CK levels in G3 affected and carrier female dogs shortly after birth may be a result of acute generalized muscle damage after the stress of whelping. It is very important to note that 32.3% of affected G3 male pups had died by 3 days of age, and the rate was significantly higher than that of normal dogs. Actually, it has been reported that 28.0% or 45.5% CXMD pups died with a neonatal fulminant form within the first 2 weeks after birth [15, 18]. Although the cause has not been fully elucidated, acute respiratory failure might be associated with the pathogenesis of the early death because involvement of the diaphragm muscle was seen in neonatal fulminant CXMD pups [19] as well as in affected G3 dogs at three days after birth (**Fig. 5E**). The stress of whelping is one factor that may exacerbate involvement of the diaphragm. Moreover, Nguyen et al. reported selective involvement of the diaphragm muscle in neonatal CXMD pups, and they found that anterior tibial muscle damage was not more severe than that of the diaphragm muscle [19]. In affected G3 dogs, a similar selec-

tive pattern was observed at the neonatal stage (**Fig. 5E and 6D**). It is very intriguing to note that genetic variation of sire may influence on the neonatal phenotypes of dystrophic dogs, since the same carrier produced different types of dystrophic pups: neonatal fulminant or less severe dystrophic pups.

The serum CK levels in G3 affected and carrier female dogs increased again at 2 months of age. Onset of clinical symptoms, such as gait and mobility disturbances and muscle atrophy, were definite from 2 months of age in affected G3 males (**Fig. 4A-E**). The onset of the disease might be closely related to the second peak of serum CK that we found in affected G3 dogs. The period of around 2 months of age corresponds to canine socialization for developing spontaneous activities after the weaning [20]. It is, therefore, possible that the increase in activity of pups may effect on an elevation of serum CK levels and on the onset of clinical symptoms. Valentine et al. reported that the age of onset of muscle involvement in CXMD dogs was from 8 to 10 weeks of age [4, 15]. Those results were largely consistent with the data on our affected G3 dogs. On the other hand, they also reported that the disease severity in affected beagle-crossed dogs was milder than that in CXMD dogs around the age of 8 weeks [15]. The same criteria could be required to evaluate and compare affected G3 dogs with CXMD dogs.

The feeding difficulty and jaw joint contracture were apparent from 4 months of age (**Fig. 4F-I**). At 6 months of age, histopathological findings of diaphragm (**Fig. 5F**) and anterior tibial (**Fig. 6F**) muscles in affected G3 male dogs were compatible with those in CXMD dogs at 6 months of age [21]. All affected G3 dogs at the age of 12 months showed severe macroglossia and hypertrophy of the sublingual muscles (**Fig. 7B**). Degeneration of tongue muscle fibers has been noted as early as the neonatal stage in CXMD [18, 19], although we have not confirmed that. Elucidation of tongue and sublingual muscle involvement in dystrophic dogs is indispensable, because dysphagia is now one of the major symptoms in older DMD patients [22, 23].

Finally, we here showed the characteristics of G3 CXMD$_J$, and especially emphasized the particular change of serum CK levels with age, not only in G3 CXMD$_J$ but also in female carrier dogs. The extremely high CK values we found in neonatal dystrophic dogs may reflect respiratory muscle damage due to stress during whelping. These findings in G3 CXMD$_J$ dogs were similar to those in CXMD dogs; therefore, CXMD$_J$ is a useful model for investigation of the pathogenesis of and development of therapies for dystrophin-deficient muscular dystrophy, DMD.

Acknowledgements

We thank Naoko Yugeta, D.V.M. (School of Veterinary Medicine, Azabu University) for advising on the healthy care of dogs and also thank Hideki Kita, Shinichi Ichikawa, Yumiko Yahata, and Kazue Kinoshita (JAC, Inc., Tokyo) for keeping of dogs. This study was supported by Grants-in-Aid for Research on Nervous and Mental Disorders (13B-1, 16B-2) and Health Sciences Research Grants for Research on Psychiatric and Neurological Diseases and Mental Health (H12-kokoro-025, H15-kokoro-021), the Human Genome and Gene Therapy (H13-genome-001, H16-genome-003) from the Ministry of Health, Labor and Welfare of Japan, and Grants-in-Aid for Scientific Research from the Ministry of Education, Science, Sports and Culture of Japan (to Y.S. and S.T.).

References

1. Moser H. Duchenne muscular dystrophy: pathogenetic aspects and genetic prevention. Hum Genet 1984;66:17-40.
2. Koenig M, Hoffman EP, Bertelson CJ, et al. Complete cloning of the Duchenne muscular dystrophy (DMD) cDNA and preliminary genomic organization of the DMD gene in normal and affected individuals. Cell 1987;50:509-17.
3. Bulfield G, Siller WG, Wight PA, et al. X chromosome-linked muscular dystrophy (*mdx*) in the mouse. Proc Natl Acad Sci USA 1984;81:1189-92.
4. Valentine BA, Cooper BJ, Cummings JF, et al. Progressive muscular dystrophy in a golden retriever dog: light microscope and ultrastructural features at 4 and 8 months. Acta Neuropathol (Berl) 1986;71:301-10.
5. Cooper BJ, Winand NJ, Stedman H, et al. The homologue of the Duchenne locus is defective in X-linked muscular dystrophy of dogs. Nature 1988;334:154-6.
6. Kornegay JN, Tuler SM, Miller DM, et al. Muscular dystrophy in a litter of golden retriever dogs. Muscle Nerve 1988;11:1056-64.
7. Valentine BA, Winand NJ, Pradhan D, et al. Canine X-linked muscular dystrophy as an animal model of Duchenne muscular dystrophy: a review. Am J Med Genet 1992;42:352-6.
8. Shelton GD, Engvall E. Canine and feline models of human inherited muscle diseases. Neuromuscul Disord 2005; 15:127-38.
9. Shimatsu Y, Katagiri K, Furuta T, et al. Canine X-linked muscular dystrophy in Japan (CXMD$_J$). Exp Anim 2003;52:93-7.

10. Yasuda S, Townsend D, Michele DE, et al. Dystrophic heart failure blocked by membrane sealant poloxamer. Nature 2005;436:1025-9.
11. Yoshimura M, Sakamoto M, Ikemoto M, et al. AAV vector-mediated microdystrophin expression in a relatively small percentage of mdx myofibers improved the mdx phenotype. Mol Ther 2004;10:821-8.
12. Dezawa M, Ishikawa H, Itokazu Y, et al. Bone marrow stromal cells generate muscle cells and repair muscle degeneration. Science 2005;309:314-7.
13. Dell'Agnola C, Wang Z, Storb R, et al. Hematopoietic stem cell transplantation does not restore dystrophin expression in Duchenne muscular dystrophy dogs. Blood 2004;104:4311-8.
14. Wilton SD, Honeyman K, Fletcher S, et al. Snapback SSCP analysis: engineered conformation changes for the rapid typing of known mutations. Hum Mutat 1998;11:252-8.
15. Valentine BA, Cooper BJ, de Lahunta A, et al. Canine X-linked muscular dystrophy. An animal model of Duchenne muscular dystrophy: clinical studies. J Neurol Sci 1988;88:69-81.
16. Kornegay JN, Bogan DJ, Bogan JR, et al. Contraction force generated by tarsal joint flexion and extension in dogs with golden retriever muscular dystrophy. J Neurol Sci 1999;166:115-21.
17. Bartlett RJ, Winand NJ, Secore SL, et al. Mutation segregation and rapid carrier detection of X-linked muscular dystrophy in dogs. Am J Vet Res 1996;57:650-4.
18. Valentine BA, Cooper BJ. Canine X-linked muscular dystrophy: selective involvement of muscles in neonatal dogs. Neuromuscul Disord 1991;1:31-8.
19. Nguyen F, Cherel Y, Guigand L, et al. Muscle lesions associated with dystrophin deficiency in neonatal golden retriever puppies. J Comp Pathol 2002;126:100-8.
20. Seksel K. Puppy socialization classes. Vet Clin North Am Small Anim Pract 1997;27:465-77.
21. Valentine BA, Cooper BJ, Cummings JF, et al. Canine X-linked muscular dystrophy: morphologic lesions. J Neurol Sci 1990;97:1-23.
22. Jaffe KM, McDonald CM, Ingman E, et al. Symptoms of upper gastrointestinal dysfunction in Duchenne muscular dystrophy: case-control study. Arch Phys Med Rehabil 1990;71:742-4.
23. Willig TN, Paulus J, Lacau Saint Guily J, et al. Swallowing problems in neuromuscular disorders. Arch Phys Med Rehabil 1994;75:1175-81.

American Journal of Pathology, Vol. 166, No. 6, June 2005

Musculoskeletal Pathology

Participation of Bone Marrow-Derived Cells in Fibrotic Changes in Denervated Skeletal Muscle

Yasushi Mochizuki,*† Koichi Ojima,* Akiyoshi Uezumi,* Satoru Masuda,* Kotaro Yoshimura,† and Shin'ichi Takeda*

From the Department of Molecular Therapy, National Institute of Neuroscience, National Center of Neurology and Psychiatry, Ogawa-higashi-cho, Kodaira, Tokyo; and the Department of Plastic and Reconstructive Surgery,† Graduate School of Medicine, The University of Tokyo, Hongo, Bunkyo-ku, Tokyo, Japan*

In denervated skeletal muscle, mononuclear interstitial cells accumulate in the perisynaptic regions before fibrotic change occurs. These cells are currently considered to be fibroblasts that originate from muscle tissue. However, when we denervated hind limbs of GFP-bone marrow chimeric mice by excising the sciatic nerve unilaterally, many bone marrow-derived cells (BM-DCs) infiltrated the interstitial spaces and accumulated in the perisynaptic regions, peaking 14 days after denervation. They accounted for nearly one-half of the increase in mononuclear interstitial cells. Although BM-DCs did not incorporate into satellite cells, immunohistochemical and FACS analyses revealed that BM-DCs were both CD45 and CD11b positive, indicating that they were of macrophage/monocyte lineage. BrdU staining showed inactive proliferation of BM-DCs. Reverse transcriptase-polymerase chain reaction of mononuclear cells isolated by FACS revealed that BM-DCs did not express type I collagen or tenascin-C; however, they did express transforming growth factor-β1, suggesting that they regulate the fibrotic process. In contrast, muscle tissue-derived interstitial cells expressed type I collagen and tenascin-C, suggesting that these populations were the final effectors of fibrosis. These findings identify elementary targets that may regulate the migration, homing, differentiation, and function of BM-DCs, leading to amelioration of the excessive fibrosis of denervated skeletal muscle. *(Am J Pathol 2005, 166:1721–1732)*

Fibrotic change is often observed after subacute or chronic inflammation, and severe fibrosis of a vital organ such as the lung, liver, or kidney is sometimes fatal. Denervated skeletal muscle tissue also exhibits persistent fibrotic change, which is accompanied by muscle fiber atrophy. This fibrosis may obstruct the recovery of atrophied muscle fibers even after reinnervation.

The number of mononuclear interstitial cells increases before fibrotic change in denervated skeletal muscle,[1,2] but labeling peripheral blood cells with radioisotopes demonstrated that the increased interstitial cells were not derived from the circulatory system.[3] These additional interstitial cells have been identified morphologically by electron microscopy as fibroblasts because they have much rough endoplasmic reticulum in their cytoplasm, actin filaments in their processes, and collagen fibers around them.[4]

With the accumulation of interstitial cells in the perisynaptic regions, increased expression of several ECMs such as tenascin-C, fibronectin, neural cell adhesion molecule (N-CAM), and heparan sulfate proteoglycans are observed in denervated skeletal muscle.[5] According to an *in vitro* study, the accumulating interstitial cells are thought to have produced these ECMs.[6] Despite all of these findings, however, whether these interstitial cells are homogeneous or heterogeneous, their definition or identification by cell surface antigens and their roles *in vivo* are still unknown.

Recently, the incorporation of bone marrow-derived cells (BM-DCs), including mesenchymal stem cells[7] or side population cells,[8] into regenerating muscle[9] or dystrophic skeletal muscle[10] was noted. Transplantation of bone marrow cells from GFP transgenic mice allowed the identification of BM-DCs in the recipient mice. Participa-

Supported by the Center of Excellence, Research on Nervous and Mental Disorders (grants-in-aid 10B-1 and 13B-1), the Ministry of Health, Labor, and Welfare of Japan, Research on the Human Genome and Gene Therapy (Health Sciences research grants H10-genome-015 and H13-genome-001), a grant-in-aid for Scientific Research (B) from the Ministry of Education, Science, Sports, and Culture of Japan, and a Research Fellowship from the Japan Society for the Promotion of Science (to K.O.).

Accepted for publication February 15, 2005.

Address reprint requests to Shin'ichi Takeda, MD, PhD, Department of Molecular Therapy, National Institute of Neuroscience, National Center of Neurology and Psychiatry, 4-1-1 Ogawa-higashi-cho, Kodaira, Tokyo 187-8502, Japan. E-mail: takeda@ncnp.go.jp.

tion of BM-DCs was reported not only in the regeneration process, but also in atherosclerotic or fibrotic lesions.[11–13] These findings suggest that regulating migration, homing, proliferation, or differentiation of BM-DCs might lead to mitigation or prevention of these lesions.

To examine whether BM-DCs are also incorporated into pathological processes in skeletal muscle, we studied the origin of the increased interstitial cells in denervated skeletal muscle by using a bone marrow chimeric animal. Here, using GFP bone marrow chimeric mice, we show for the first time that a considerable proportion of these interstitial cells are bone marrow-derived, ie, they are not of traditional fibroblast lineage but of macrophage/monocyte lineage, and that they are a possible regulator of the muscle tissue-derived interstitial cells that might finally constitute the fibrosis.

Materials and Methods

Animals

C57BL/6J mice (B6 mice) and BALB/c mice were purchased from Nihon CLEA (Tokyo, Japan). C57BL/6J-*GFP*-transgenic mice[14] were kindly provided by Dr. Okabe (Osaka University, Japan). All procedures used on experimental animals were approved by the Experimental Animal Care and Use Committee at the National Institute of Neuroscience.

BM Chimeric Mice and Denervation

Whole bone marrow cells were collected from humeri, femurs, and tibias of 7- to 8-week-old donor GFP-transgenic mice by aspiration and flushing. Mononuclear cells were refined through 40-μm and subsequently 10-μm filters and next by centrifugation with Lympholite-M (Cedarlane, Hornby, Ontario, Canada), and then they were diluted to concentrations of 5 to 10 $\times$ 10^6 cells in 100 μl of phosphate-buffered saline (PBS). Female C57BL/6J mice (7- to 8-week old) were lethally irradiated with 9 Gy (Hitachi Medical Co., Tokyo, Japan) immediately before retro-orbital injection of the donor BM cells under general anesthesia with 0.05 mg/g (body weight) of pentobarbiturate (Nembutal). These mice were given drinking water containing 1 mg/ml of ampicillin for 2 weeks after the transplantation.

Twelve weeks after the transplantation, the left sciatic nerve of the bone marrow recipients was excised for nearly the full length of the thigh (approximately 10 mm) from a small incision (approximately 4 mm) made in the mid-lateral thigh under general anesthesia and a surgical microscope (Olympus, Tokyo, Japan). The mice were sacrificed 1 day (day 1) to 4 months (day 112) after denervation by cervical dislocation under general anesthesia. The left gastrocnemius muscle was excised for analysis. The right gastrocnemius muscle served as the control sample. Bone marrow cells simultaneously collected from the femur were purified and then were analyzed by FACS (FACS VantageSE flow cytometer; Falcon, Franklin Lakes, NJ) to determine the bone marrow chimerism as a percentage of GFP-positive cells.

Immunohistochemistry

Muscle samples were fixed with 4% formaldehyde in PBS for 30 minutes and washed with 10% sucrose in PBS for 6 hours and then with 20% sucrose overnight. The samples were then soaked in OCT compound and frozen in isopentane cooled in liquid nitrogen. Serial cryostat sections (10 μm thick) were stained with hematoxylin and eosin (H&E) or immunohistochemically as described below. Sections were washed with PBS for 30 minutes, blocked with 1% bovine serum albumin, and then were reacted with first (37°C, 1 hour) and second (room temperature, 30 minutes) antibodies. Nuclei were stained with TOTO-3 (room temperature, 10 minutes). After staining, the sections were examined under a confocal laser-scanning microscope (Leica TCS SP; Leica, Heidelberg, Germany). To count GFP-positive cells, five randomly selected high-power fields of neuromuscular junction-rich and -poor areas were examined.

Western Blotting Analysis

Twenty to 40 cryostat sections of day 28 or day 112 gastrocnemius muscles were dissolved with 4 volumes (w/v) of sample buffer (10% SDS, 70 mmol/L Tris-HCl (pH 6.7), 10 mmol/L EDTA, and 5% β-mercaptoethanol), boiled for 5 minutes, and then cooled on ice. The samples were centrifuged by 14,500 rpm for 15 minutes, and then the supernatants were collected. The amounts of harvested protein were determined based on OD 595 using Bradford solution. Equal amounts of protein (30 μg each) underwent electrophoresis (200V, 45 minutes) on READYGELS J (7.5%; Bio-Rad, Tokyo, Japan). After semidry blotting was performed (242mA, 1 hour), the membrane was reacted with first (4°C, overnight) and horseradish peroxidase-conjugated second (room temperature, 1 hour) antibodies. The signals were analyzed using Lumi-Imager F1 (Roche Molecular Biochemicals, Tokyo, Japan).

FACS Analysis of Muscle Mononuclear Cells

The visible nerves, blood vessels, and tendons of the whole hind limb muscle of the denervated or intact side were removed with microsurgical forceps under a dissection microscope. Trimmed muscles were minced with scissors and then treated with 0.2% collagenase type 2 under stir for 40 minutes at 37°C. Digested muscles were filtered through a 100-μm and subsequently a 40-μm filter, and then red blood cells were removed by treatment with 0.8% NH_4Cl. The mononuclear cells obtained were suspended in 100 μl of PBS and reacted with antibodies. The first antibody (on ice, 30 minutes) was allophycocyanin-conjugated anti-CD45, phycoerythrin (PE)-conjugated anti-CD11b, or biotin-conjugated anti-CD44. The second reagent for the biotin-conjugated anti-CD44 antibody was PE-conjugated streptavidine (on ice, 15

minutes). Finally, the samples were washed with PBS, dissolved in 1 ml of PBS with 2% bovine serum albumin, and analyzed by FACS.

BrdU Staining

Mice at day 4 were injected intraperitoneally with 50 μg/g body weight of BrdU in 200 μl of PBS. Two hours after the injection,[15] the mice were sacrificed by cervical dislocation. Fixation of the muscle sample was the same as that for immunohistochemistry. Cryostat sections (5 μm thick) were stained with chicken anti-GFP antibody and subsequently fluorescein isothiocyanate-conjugated anti-chicken IgG antibody. Next, after fixation of GFP with 2% formaldehyde, DNA was denatured by 2 N HCl and neutralized by 0.1 mol/L sodium 4-borate (pH 8.5). Then, BrdU staining with anti-BrdU antibody and subsequently Alexa Fluor 568-conjugated goat anti-mouse IgG was performed. The sample was examined under a confocal laser microscope.

Apoptotic Cell Detection

Apoptotic cells were detected on cryostat sections using ApopTag^R Red *In Situ* Apoptosis Detecting kit (Chemicon International Inc.) according to manufacturer's instructions. Briefly, cyostat sections were prepared as described in immunohistochemistry section. Next, GFP staining and fixation was performed as described under BrdU Staining. After being postfixed and permeabilized with pre-cooled (−20°C) mixture of ethanol and acetic acid (2:1), the sections were reacted with digoxigenin-labeled nucleotides under the presence of terminal deoxynucleotidyl transferase. Then, the sections were reacted with rhodamine-conjugated sheep polyclonal anti-digoxigenin antibody. Nuclei were stained with TOTO-3. Sections were examined under a confocal laser microscope.

Reverse Transcriptase-Polymerase Chain Reaction (RT-PCR)

Three fractions of mononuclear cells, GFP positive, GFP negative/CD44 positive, and GFP negative/CD44 negative, from four day 28 mice were isolated by FACS and diluted in PBS. Total RNA from 1 × 10^4 cells of each population was isolated using RNeasy (Qiagen, Tokyo, Japan) according to the manufacturer's instructions and reverse transcribed using oligo dT primers with a total reaction volume of 30 μl. The reverse transcription program was 25°C for 10 minutes, 48°C for 30 minutes, and then 95°C for 5 minutes. Polymerase chain reaction was performed using 3 μl of each RT product (cDNA), with a total reaction volume of 20 μl. The PCR thermal cycle was 94°C for 3 minutes, then 40 cycles (or 30 cycles for transforming growth factor (TGF)-β1) of 94°C for 15 seconds, 60°C for 30 seconds, and 72°C for 30 seconds, and finally 72°C for 5 minutes.

The primers for PCR were type I collagen (413-bp product) sense (5′-GTGAACCTGGCAAACAAGGT-3′) and antisense (5′-CTGGAGACCAGAGAAGCCAC-3′), MMP-14 (308-bp product) sense (5′-ACAAAGATGCCCCCTCAACC-3′) and antisense (5′-GCTTCGTCAAACCAGTGC-3′), MMP-3 (391-bp product) sense (5′-TTCTCCAGGATCTCTGAAGGAGAGG-3′) and antisense (5′-ATTTGGTGGGTTACCACGAGGACATC-3′), tenascin-C (355-bp product) sense (5′-GCCTCAACAACTGCTACAATCGTG-3′) and antisense (5′-TCAGCCCCTGTGAACCCATC-3′), α-smooth muscle actin (α-SMA) (240-bp product) sense (5′-GAGAAGCCCAGCCAGTCG-3′) and antisense (5′-CTCTTGCTCTGGGCTTCA-3′), and TGF-β1 (431-bp product) sense (5′-CTAATGGTGGACCGCAACAAC-3′) and antisense (5′-CGGTTCATGTCATGGATGGTG-3′). These primers were obtained from Qiagen. Primers for β-actin (540-bp product) were sense (5′-GTGGGCCGCTCTAGGCACCAA-3′) and antisense (5′-CTCTTTGATGTCACGCACGATTTC-3′). As positive controls for these primers, RNA samples from 8-week-old mouse mammary gland were used for MMP-3 and from mouse embryo (day 13) were used for the rest.

Antibodies and Chemicals

Collagenase type 2 was from Worthington Biochemical Corp. (Lakewood, NJ). Allophycocyanin-conjugated rat anti-mouse CD45 antibody (clone 30-F11), rat anti-mouse CD31 antibody (clone MO76917), PE-conjugated rat anti-mouse CD11b antibody (clone M1/70), and mouse anti-BrdU antibody (clone MO76134) were from Becton Dickinson (San Diego, CA). Rat biotin-conjugated anti-mouse CD44 antibody (clone KM201) was from Southern Biotechnology Associates, Inc. (Birmingham, AL). Rat anti-mouse laminin-α2 antibody (clone 4H8–2) was from Alexis Corp. (San Diego, CA). Rabbit polyclonal anti-mouse type I collagen antibody (for immunohistochemistry) was from Biogenesis Inc. (Kingston, NH). Rat anti-mouse tenascin-C antibody (clone Mtn12)[16] was kindly provided by Prof. Ekblom (Department of Animal Physiology, Uppsala University, Uppsala, Sweden). Goat polyclonal anti-rat C/EBPα antibody, rabbit polyclonal anti-m-cadherin antibody, goat polyclonal anti-mouse collagen α2 type I antibody (for Western blotting analysis), and rabbit polyclonal anti-human TGF-β1 antibody were from Santa Cruz Biotechnology (Santa Cruz, CA). Rabbit polyclonal anti-human α-SMA antibody was from Lab Vision Corp. (Fremont, CA). Rat anti-mouse N-CAM (clone MAB310) and chicken polyclonal anti-GFP antibody and ApopTag Red *In Situ* Apoptosis Detection kit were from Chemicon International Inc. (Temecula, CA). Alexa Fluor 594-conjugated goat anti-rat IgG antibody, Alexa Fluor 568-conjugated goat anti-rabbit IgG antibody, Alexa Fluor 594-conjugated donkey anti-goat IgG antibody, Alexa Fluor 568-conjugated goat anti-mouse IgG antibody, Alexa Fluor 594-conjugated α-bungarotoxin, and TOTO-3 iodide (642/660) were from Molecular Probes (Eugene, OR). Fluorescein isothiocyanate-conjugated donkey polyclonal anti-

chicken IgG antibody was from Jackson Immuno Research Laboratories (West Grove, PA). Horseradish peroxidase-conjugated rabbit anti-goat IgG antibody was from Zymed Laboratories Inc. (San Francisco, CA). The RNeasy Micro kit was from Qiagen.

TaqManR Reverse Transcription Reagents were from Roche Molecular Systems, Inc. (Branchburg, NJ). The Mouse β-actin Control Amplimer set was from CLONTECH Laboratories, Inc. (Palo Alto, CA). ECL Western Blotting Detection Reagents were from Amersham Biosciences (Little Chalfont, Buckinghamshire, United Kingdom).

Statistical Analysis

Results were expressed as means ± SD. For comparison between any two groups, Welch's *t*-test was applied based on results of the data analysis by F-test. A P value of less than 0.01 was considered to indicate statistical significance.

Results

Establishment of GFP BM Chimeric Mice

Fifty-three mice received bone marrow transplantation. Of these, 45 mice were sacrificed and analyzed. The mean bone marrow chimerism at the time of sampling was 88.5 ± 7.9%. One mouse died of unknown cause 16 days after the bone marrow transplantation. Five mice were excluded from the study because of scar contraction of the hind limb due to irradiation. Two mice died of deep anesthesia.

Muscle Fiber Atrophy, Increased Interstitial Cells, and Fibrosis in Denervated Muscle

To verify the condition of denervation, the decrease of the diameter of gastrocnemius muscle fibers was examined by analyzing immunohistochemical images. On the denervated side (left), the diameter was significantly decreased 4 days after denervation (day 4; Figure 1). Denervation was also ascertained by observation of separate unconnected stumps of the cut sciatic nerve. On H&E stain, an increase in the number of interstitial mononuclear cells was observed from day 4. They accumulated in perisynaptic regions, as reported in the literature.[1,2]

From day 14, progressive fibrosis was detected by H&E staining. Fibrotic change was also examined by immunostaining for type I collagen (Figure 3, c and d). Fatty change was not observed in C57BL/6J mice, at least up to 4 months after the denervation (day 112). In contrast, the hind limb muscles of BALB/c mice showed fatty change from 1 month after denervation (day 28; data not shown). This difference in phenotypic expression may be interpreted as the influence of background strain.

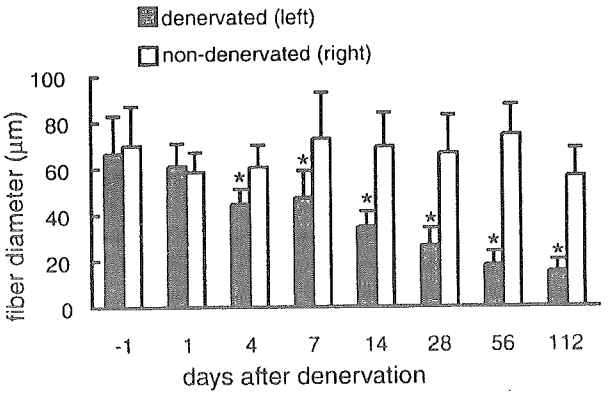

Figure 1. Decrease of muscle fiber diameter in denervated muscle. Diameters of muscle fibers of both denervated (**left, gray bar**) and nondenervated (**right, white bar**) gastrocnemius muscle were measured before denervation (−1) and 1 to 112 days after denervation. Bars represent the means ± SD of 50 fibers. $^*P < 0.01$.

BM-DCs Accumulated in the Perisynaptic Region

On day 4, many GFP-positive BM-DCs had entered the denervated (left) gastrocnemius muscle, mainly at the external fascia and perimysium (Figure 2, a and b). BM-DCs then faded out of these regions from day 7, but at the same time they appeared on the endomysium of each muscle fiber and gradually accumulated in the perisynaptic regions (Figure 3a). The time course of the appearance of BM-DCs in the perisynaptic region is shown in Figure 4, a and b. From day 4, BM-DCs significantly increased in the perisynaptic region to reach a maximum around days 14 to 28; thereafter, they gradually decreased. The initial accumulation at the perimysium on day 4 was excluded from this analysis. Distortions in the arrangements and decreases in the number of NMJs were also observed from 2 months after the denervation (day 56) and were more apparent on day 112 (Figure 3b).

When we compared the high-magnification fluorescent images of BM-DCs with that of H&E staining, BM-DCs accounted for considerable part of the interstitial mononuclear cells (Figure 2, c and d). Quantitative analysis showed that BM-DCs accounted for around 43% of the interstitial cells on day 4, 41% on day 14, and 39% on day 28, respectively (Figure 5a). However, as long as we considered only the shape of these increased interstitial cells, BM-DCs and muscle tissue-derived cells (MT-DCs) were indistinguishable under the microscope, and they were spindle or stellate shaped, as reported in the literature.[4]

BM-DCs Co-Localized with Expression of ECMs

Some fibrosis-related components of ECMs are known to accumulate around the perisynaptic regions of denervated skeletal muscle.[5] We examined whether BM-DCs co-localize with expressions of some components of ECMs. Type I collagen was detected in the perisynaptic regions in which BM-DCs were also accumulated (Figure 3, c and d). The accumulation of type I collagen was in

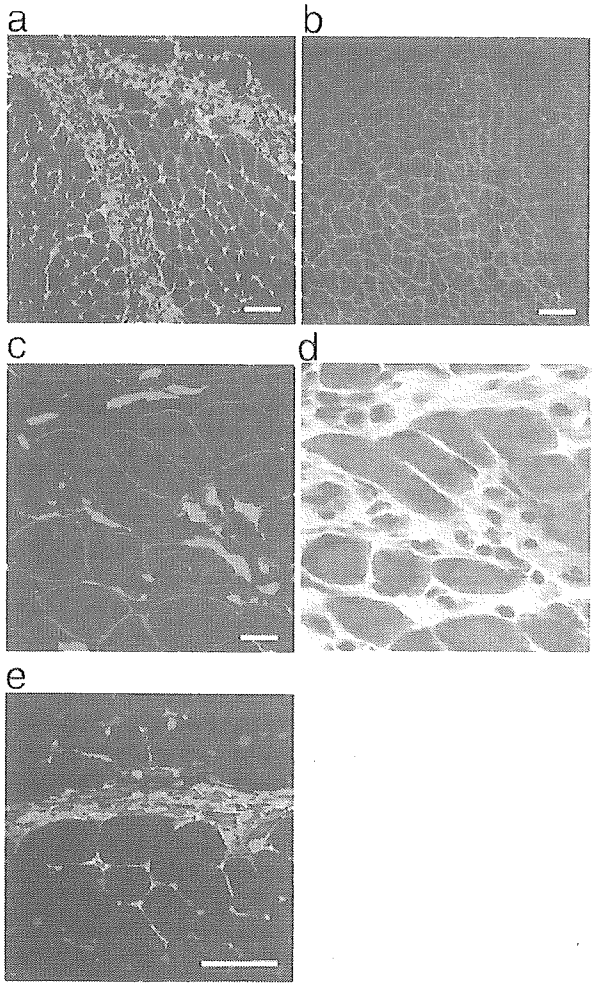

Figure 2. BM-DC infiltration into denervated muscle and co-localization with ECMs. Analysis by immunohistochemistry and H&E. **a:** Many BM-DCs (green; GFP) had infiltrated the external fascia and perimysium (green bands) and spread into the endomysium of denervated gastrocnemius muscle 4 days after denervation (day 4), whereas the nontreated side (**b**) showed no increase of BM-DCs (red; laminin-α2 representing basement membrane). Comparison at high magnification of GFP-positive cells (**c**; green) with interstitial mononuclear cells in H&E (**d**) shows that BM-DCs account for considerable part of the interstitial cells. **e:** Expression of tenascin-C (red) on day 4 at the perimysium, at which the BM-DC (green or merged with nucleus to light blue) accumulated. Within the perimysium, mononuclear MT-DCs (spindle-shaped areas with nuclei, lacking red signal) are also observed. TOTO-3 (dark blue) was used for nuclear staining. Scale bars = 100 μm (**a** and **b**), 20 μm (**c**), and 40 μm (**e**).

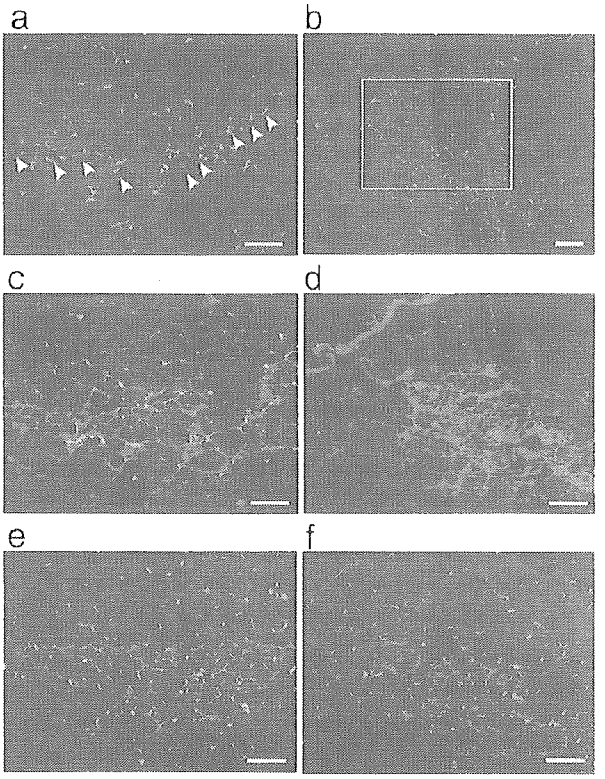

Figure 3. Accumulation of BM-DCs in the perisynaptic region and their co-localization with ECMs. Immunohistochemical analysis of day 28 (**a**, **c**, and **e**; serial sections) and day 112 (**b**, **d**, and **f**; serial sections). BM-DCs accumulated in the perisynaptic regions (**a** and **b**), co-localizing with type I collagen (**c** and **d**, red). BM-DCs also co-localized with tenascin-C on day 28 (**e**, red). Tenascin-C revealed spotted pattern on day 112, although still associating with BM-DCs (**f**, red). **Arrowheads** in **a** indicate individual NMJs (α-bungarotoxin, red). The box in **b** corresponds to the fields of **d** and **f**. Scale bars = 80 μm (**a** and **c** to **f**) and 100 μm (**b**).

accordance with the progressive fibrosis observed in H&E staining. However, immunoblotting analysis showed no evidence that total type I collagen protein had been increased in denervated entire gastrocnemius muscle compared with that of intact side (data not shown). Thus, even if there is increased synthesis of type I collagen in fibrotic lesion in denervated skeletal muscle, degradation of type I collagen may also be involved in the pathogenesis of fibrosis.[17]

The expression of tenascin-C, an anti-adhesion molecule, also accompanied the distribution of BM-DCs and appeared in the perisynaptic regions. On day 4, tenascin-C was detected around the invading BM-DCs or MT-DCs at the perimysium (Figure 2e). On day 7, tenascin-C disappeared from the perimysium, and BM-DCs also disappeared. After day 7, tenascin-C was again detected at the perisynaptic regions in which BM-DCs also accumulated (Figure 3e). This accumulation of tenascin-C might support the idea that tenascin-C appears at sites to which cells migrate, such as development, inflammation, tumorigenesis, and wound healing.[18] However, the expression pattern of tenascin-C was more distinctly restricted to each NMJ than that of type I collagen, especially on day 112 (Figure 3f). Thus, tenascin-C may initially regulate accumulation of BM-DCs at the perimysium, then in perisynaptic regions, and thereafter control, for example, the dynamic induction of regenerating axons to each NMJ. On the other hand, N-CAM[6] was uniformly distributed at each endomysium from day 4, showing no particular co-localization with BM-DCs (data not shown).

There is a possibility that BM-DCs can differentiate into particular cell lineages. Therefore, we examined several typical lineage markers. α-SMA is a marker for myofibroblasts or activated interstitial cells found in inflammatory or chronic lesions. The expression of α-SMA was not detected among BM-DCs and MT-DCs (data not shown). Whether BM-DCs incorporate into satellite cells in skeletal muscle is currently controversial.[19,20] In the present

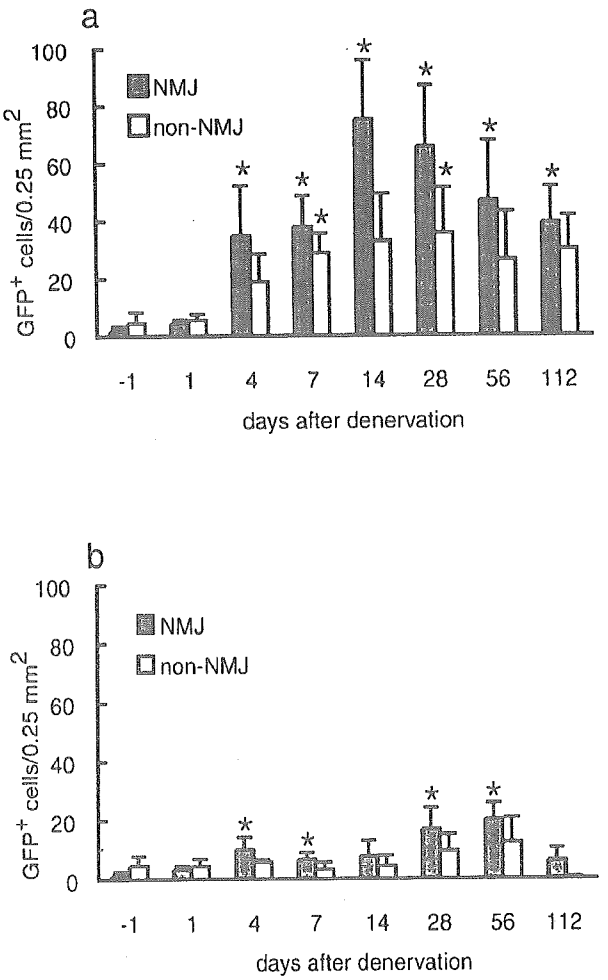

Figure 4. Increase of the BM-DCs in denervated gastrocnemius muscle. Time course of the BM-DC increase in left denervated (**a**) or right nontreated (**b**) side. Data are shown as numbers of GFP-positive cells per field (0.25 mm^2) including (**gray bars**) or excluding (**white bars**) NMJ regions. Bars represent the means ± SD of five fields. $^*P < 0.01$.

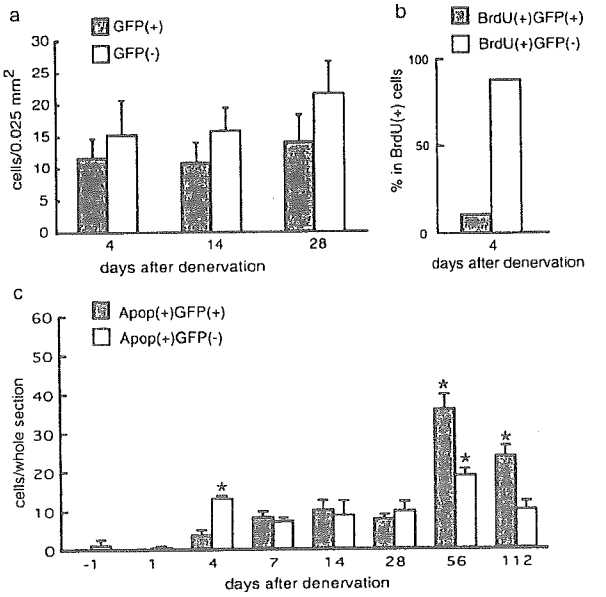

Figure 5. The ratio of BM-DCs among interstitial mononuclear cells in denervated gastrocnemius muscle and their proliferation or apoptotic activity. **a:** Numbers of BM-DCs (**gray bars**) and MT-DCs (**white bars**) around NMJs of denervated muscle. Data are shown as cell numbers per field (0.025 mm^2/field). Interstitial connective tissue was defined as tissue outside the muscle fiber basement membrane stained by laminin-α2. Mononuclear cells were defined by nuclear staining with TOTO-3. **b:** The proportion of interstitial cells (**gray bar**, GFP positive; **white bar**, GFP negative) that were BrdU positive after 2 hours of BrdU exposure in a whole cross-sectional area of gastrocnemius muscle 4 days after denervation. **c:** Time course of apoptotic activity of BM-DCs (**gray bars**) and MT-DCs (**white bars**) of denervated muscle. Data are shown as numbers of apoptotic (Apop) cells per whole muscle section. Bars represent the means ± SD of five fields (**a**) or three whole sections (**c**), respectively. $^*P < 0.01$.

study, GFP-positive satellite cell was not detected in denervated muscle. None of the other lineage markers tested, including CD31 (platelet/endothelium cell adhesion molecule-1) for vascular endothelium, neonatal myosin heavy chain for developing myofibers, and C/EBP-α for adipose cells, was detected among those interstitial cells. Thus, BM-DCs were revealed to be negative for some typical lineage markers, although sparing the possibility that they are fibroblasts.[21]

GFP-positive BM-DCs were also observed in gastrocnemius muscles of the intact side or bilateral nondenervated muscle (Figure 4, a and b). Inappropriate homing of hematopoietic or mesenchymal stem cells resulting from peripheral intravenous injection of bone marrow cells may have caused the survival of these cells. These cells may also reflect the existence of migrant, but long-term-resident, muscle interstitial cells. However, significant increase of BM-DCs in the intact side (Figure 4b) may due to sensitization via denervated leg.

BM-DCs in Denervated Skeletal Muscle Had Monocyte/Macrophage Phenotype

To investigate whether BM-DCs retain a hematopoietic lineage even in denervated skeletal muscle, we tested them for CD45 and CD11b by FACS analysis of total mononuclear cells harvested from whole denervated muscle and by immunohistochemistry of corresponding samples. On FACS analysis, at least up to day 28, the GFP-positive population was revealed to be CD45- and CD11b-positive (Figure 6, a and b). These results again showed that BM-DCs have not *trans*-differentiated into a nonhematopoietic lineage, including fibroblastic, angiogenic, myogenic, adipogenic, or neurogenic lineage, but are fundamentally of monocyte/macrophage lineage.

Next, we tried to define the migrating nature of the increased interstitial cells including BM-DCs and mononuclear MT-DCs by their CD44 expression. CD44 is an adhesive molecule known as an ECM (hyaluronan) receptor[22] that is broadly expressed on the surface of hematopoietic[23] and nonhematopoietic cells of vertebrates. CD44 is involved in lymphocyte homing, macrophage or lymphocyte activation, and tumor metastasis.[24–26] CD44 connects actin filaments with MMP-14 (membrane type 1-MMP; MT1-MMP), which is a representative of membrane type MMP,[27] or activates proMMP-2 at the forward processes (lamellipodia) of such migrating cells.[28] Put together, we expected the

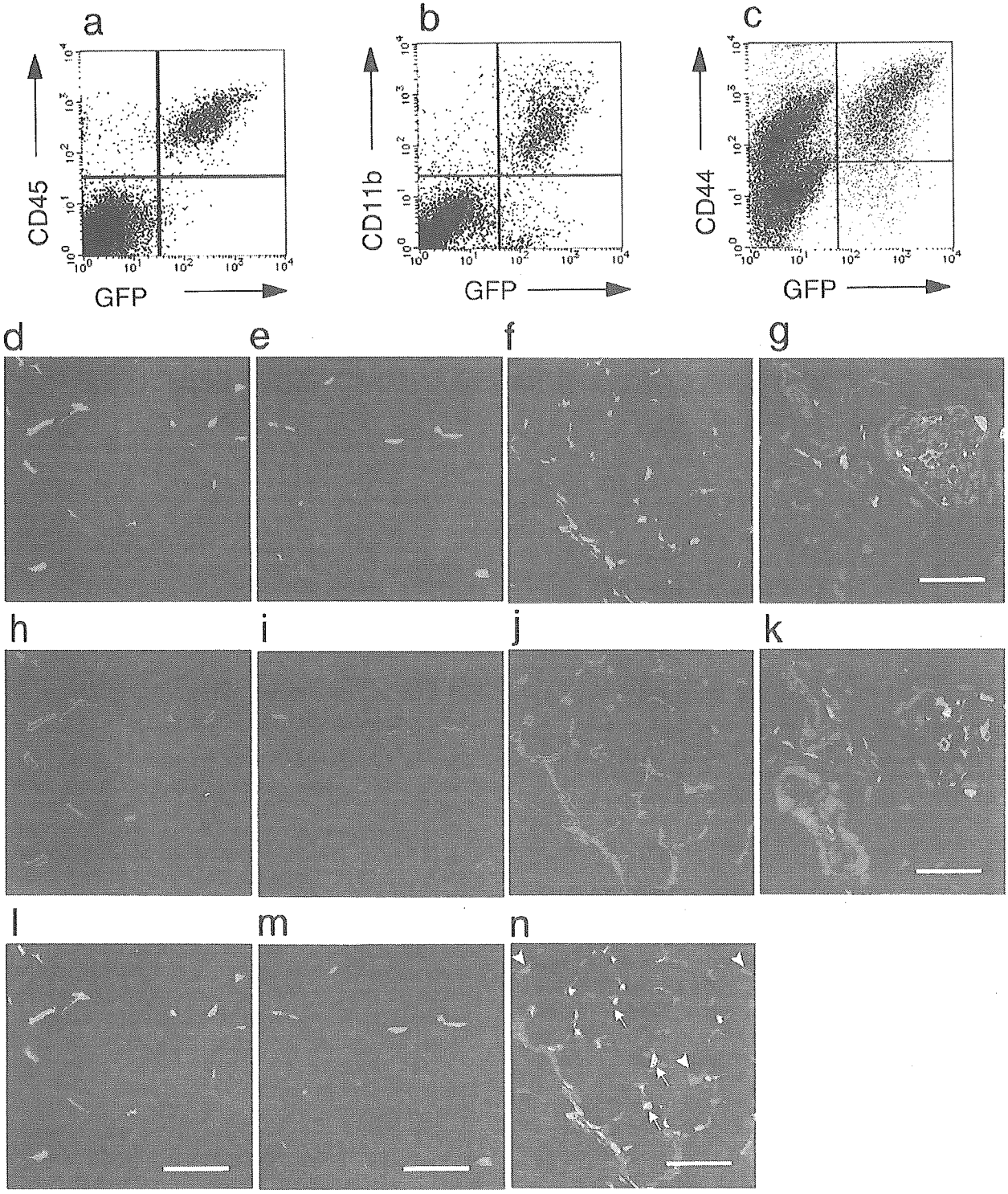

Figure 6. Flow cytometric and immunohistochemical analysis of increased mononuclear interstitial cells in denervated muscle. **a** to **c:** Mononuclear cells were isolated from gastrocnemius muscle 4, 14, and 28 days after the denervation. Following appropriate immunostaining, the cells were analyzed by flow cytometry. Representative results of analysis of isolated mononuclear cells 4 days after the denervation for GFP and CD45 (**a**), CD11b (**b**), and CD44 (**c**). **d** to **n:** Immunohistochemical analysis of BM-DCs in gastrocnemius muscle 14 days after the denervation. Almost all GFP-positive cells (**d** to **f**; green) co-stained with CD45 (**h**; red) and CD11b (**i**, red) and therefore revealed a merged expression pattern for these antigens (**l** and **m**; merged into yellow). On the other hand, CD44-positive cells (**j**; red) were GFP positive (**f**, **j**, and **n**; **arrows**) or GFP negative (**f**, **j**, and **n**; **arrowheads**). **g** and **k:** Serial sections of a neuro-vascular bundle in a gastrocnemius muscle 4 days after denervation stained for CD44 (**g**; red) or α-SMA (**k**;, red). TOTO-3 (blue) was used for nuclear staining. Scale bars = 40 μm.

increased mononuclear interstitial cells migrating to the perisynaptic regions to be CD44 positive whether they were BM-DCs or MT-DCs. Accordingly, CD44-positive mononuclear cells contained both GFP-positive and GFP-negative fractions (Figure 6c, top right and top left fractions, respectively). These fractions were supposed to reflect BM-DCs and mononuclear MT-DCs, respectively.

Immunohistochemical analysis supported those findings. Almost all BM-DCs were CD45 positive up to 2 months after the denervation (day 56; Figure 6, d, h, and l) and CD11b positive at least up to 4 months after the denervation (day 112) (Figure 6, e, i, and m, respectively). In addition, almost all interstitial mononuclear cells that might include BM-DCs and mononuclear MT-DCs were positive for CD44 at least up to day 112 (Figure 6, f, j, and n).

Observation of the posterior tibial artery revealed that vascular endothelial cells are CD44 negative (Figure 6, g and k). However, the tibial nerve trunk contained CD44-positive but GFP-negative cells, which were revealed to be Schwann cells by comparing them with a serial section stained with S-100 protein (Figure 6g; data not shown). Some of the large GFP-positive cells observed within the nerve trunk in Figure 6g may be macrophages that are involved in phagocytosis of degenerated axons.[15] Combining the mononuclear cell count with the fractional percentile of FACS-gated cells suggested that the denervated (left) gastrocnemius muscle contained around three to four times as many BM-DCs by muscle weight than the nondenervated (right) side (data not shown).

Poor Proliferation Activity of BM-DCs

There is a possibility that the GFP-positive cells observed in the denervated gastrocnemius muscle originated from muscle tissue-derived GFP-positive interstitial cells: long-term residents of skeletal muscle were found in the nondenervated side. In addition, the increase of the GFP-positive cells may depend on their proliferation by dividing or on a constant supply from the circulation system.

To answer these questions, we performed BrdU staining of denervated gastrocnemius muscle on day 4, the time point of the maximum reported proliferation activity of the increased interstitial cells.[2,3] GFP-positive interstitial cells formed only a very small minority of the BrdU-positive population in the denervated gastrocnemius muscle of day 4 (Figure 5b). Because GFP-positive cells accounted for nearly half of the increased interstitial cells in denervated gastrocnemius muscle on day 4 (Figure 5a), this result suggests poor proliferation potential of the GFP-positive population. Taking only the short life span of blood cells into consideration, it is further suggested that the majority of the increased GFP-positive cells in denervated muscle are not muscle tissue-derived dividing cells but are a bone marrow-derived and continuously supplied population.

Contribution of Apoptosis to the Decrease in Number of BM-DCs

The gradual decrease in number of BM-DCs in denervated gastrocnemius muscle observed from day 28 may be due to decreased circulating-in, increased re-circulating, or increased apoptotic activity of BM-DCs. To assess the contribution of apoptosis to the decrease in number of BM-DCs, we performed quantitative analysis of apoptotic cells in denervated gastrocnemius muscle. GFP-positive apoptotic cells significantly increased in number from day 56 ($P < 0.01$; Figure 5c). The result suggests that increased apoptotic activity of BM-DCs contributed to the gradual decrease in number of BM-DCs in denervated skeletal muscle. Although implication of the increased apoptotic activity of GFP-negative cells (MT-DCs) on day 4 (Figure 5c) is unclear, apoptotic activity of MT-DCs generally followed that of BM-DCs, indicating cooperative cellular rolls among these populations.

BM-DCs Expressed TGF-β1

To distinguish the functional roles of BM-DCs and MT-DCs, we studied the gene expression patterns of these populations by RT-PCR (Figure 7a). Denervated skeletal muscle of day 28 mice was chosen because many BM-DCs had accumulated in the perisynaptic region at the date. As controls, bilateral intact hind limb muscles of bone marrow chimeric mice were used instead of those of the contra-lateral side of the denervated limb to exclude the possibility of any compensative up- or down-regulation of the genes.

In denervated muscle, the CD44-positive MT-DCs, which may reflect muscle tissue-derived mononuclear cells and Schwann cells (as shown in Figure 6g), mainly expressed type I collagen and tenascin-C, suggesting that this population contains fibroblasts as the main effector of fibrosis (Figure 7a, lane 2). In contrast, BM-DCs did not express type I collagen or tenascin-C; instead, they dominantly expressed TGF-β1, a principal growth factor known to promote fibrosis in persistent inflammation or to induce the synthesis of tenascin-C *in vitro* (Figure 7a, lane 1).[29] Immunohistochemical analysis showed dominant production of TGF-β1 protein by a portion of BM-DCs (Figure 7, b to d). TGF-β1 expressions by the CD44-positive MT-DCs, which potentially include fibroblasts, were not observed by RT-PCR (Figure 7a, lane 2) or immunohistochemically. However, slight to moderate amplification of TGF-β1 was detected from MT-DCs when PCR was performed by 40 cycles, in accordance with the common establishment that virtually all fibroblasts express TGF-β1 (data not shown). Despite being considered to only reflect vascular endothelial cells as shown in Figure 6k and therefore to express no particular molecules studied here, the CD44-negative MT-DCs also expressed type I collagen and tenascin-C (Figure 7a, lane 3).

We examined whether MMP- 3 (stromelysin-1), one of the soluble MMPs known to breakdown the largest variety